Three-quasiparticle states analysis in odd-mass lead isotopes

N. Sandulescu* and A. Insolia

Dipartimento di Fisica, Università di Catania and Istituto Nazionale di Fisica Nucleare, I-95129 Catania, Italy

J. Blomqvist and R. J. Liotta

Manne Siegbahn Institute, S-10405 Stockholm, Sweden

Three quasiparticle excitations for odd-even lead isotopes in the mass region $197 \leq A \leq 203$ are calculated using a realistic two-body interaction. The analysis is performed in a correlated basis constructed by the tensor product of one times two quasiparticle states. Good agreement with available experimental data is found. The one phonon approximation of the weak coupling model is also analyzed.

PACS number(s): 21.60.−n, 21.60.Jz, 27.80.+w

I. INTRODUCTION

In the last years the level schemes of neutron-deficient odd-mass lead isotopes have been investigated up to high spin excitations and for many holes outside the magic core of ^{208}Pb [1–9]. The three-quasiparticle (3qp) states have been analyzed mainly within the framework of the Tamm-Dancoff approximation (TDA) [10] using a surface delta interaction with pairing subtraction [11]. Some of the levels in individual isotopes could thus be described [1–5], but a complete calculation of 3qp states with a single set of parameters in all lead isotopes has not been achieved so far. The main difficulty that one faces in these microscopic calculations is related to the dimensions of the TDA matrices, which hinder the application of the formalism beyond a few particles outside the core. This can be overcome by using the BCS approximation, but then one violates the number of particle conservation symmetry and spurious states appear by using the TDA formalism. To deal with this problem, in Ref. [12] a generalization of the multistep shell-model method [13] was presented. Within this generalization the spurious state is decoupled from the rest of the spectrum by calculating two-quasiparticle states by means of the quasirandom phase approximation (QRPA). The spurious state is easily recognized because it is a state 0^+ with energy $\omega(0_1^+)=0$. After the two-quasiparticle states have thus been calculated one proceeds to calculate systems with an increasing number of quasiparticles in several steps. The method was thus called [12] the quasiparticle multistep shell-model method (QMSM). Within the QMSM a good description of four-quasiparticle excitations has been obtained for even-even lead isotopes [12].

The aim of this paper is to extend the QMSM to the case of 3qp excitations. All parameters entering the calculation will be taken from the previously calculated even-even nuclei. Thus a unified description of lead isotopes is intended.

The formalism is presented in Sec. II, applications are in Sec. III, and a summary and conclusions are in Sec. IV.

II. FORMALISM

Within the QMSM one solves a many-quasiparticle system in several steps. Starting with a general two-body interaction one writes the Hamiltonian in a quasiparticle representation by using the Bogoliubov transformation. One then evaluates the quasiparticle energies and BCS occupation probabilities by requiring an average number of particle conservation and the condition $H_{20}=0$, as usual. In the next step one calculates two-quasiparticle states by means of the QRPA. The spurious state 0^+, which appears as a result of the breaking of the particle number gauge symmetry, is decoupled from the rest of the spectrum just by neglecting it when building the QMSM bases for more complex excitations. The two-quasiparticle states thus evaluated are used to construct correlated bases for systems with more quasiparticles. The calculated quantities corresponding to those systems are, in turn, used to calculate more complex systems. One can say that at each step of the QMSM procedure one constructs building blocks to be used in the following steps. A detailed presentation of the method can be found in Ref. [12], where two- and four-quasiparticle states in the lead region were studied.

In our 3qp case we build the QMSM basis as the tensor product of one times 2qp states, i.e.,

$$|\alpha_3\rangle = \Gamma^+(\alpha_3)|0\rangle , \tag{2.1a}$$

$$\Gamma^+(\alpha_3) = \sum_{i\alpha_2} X(i\alpha_2;\alpha_3)[\alpha_i^+ \Gamma^+(\alpha_2)]_{\alpha_3} , \tag{2.1b}$$

where

$$\Gamma^+(\alpha_2) = \sum_{i \leq j} X(ij;\alpha_2)\frac{(\alpha_i^+ \alpha_j^+)_{\alpha_2}}{\sqrt{(1+\delta_{ij})}} . \tag{2.1c}$$

We use the same symbol (X) for the two- and three-quasiparticle amplitudes. But the arguments clearly indicate which systems are involved and no confusion should

*Permanent address: Institute of Atomic Physics, Bucharest Magurele, POB MG-6, Romania.

arise from this coincidence. The backward-going amplitudes in the QRPA 2qp states are very small in comparison with the forward-going amplitudes [12], except for the spurious state 0_1^+ which we exclude from the calculation. Therefore we neglect the backward-going amplitudes, and the normalization of the states is performed according to the TDA metric,

$$\sum_{i \leq j} X^*(ij;\alpha_2)X(ij;\beta_2)=\delta_{\alpha_2\beta_2} \ . \tag{2.1d}$$

In an overcomplete basis the wave-function amplitudes are not well-defined quantities. But the projections of basis vectors on the physical state are well defined in all cases. In our 3qp case that projection is

$$F(i\alpha_2;\alpha_3)=\langle\alpha_3|[\alpha_i^+\Gamma^+(\alpha_2)]_{\alpha_3}|0\rangle \ . \tag{2.2}$$

The angle θ between the calculated state $|\alpha_3\rangle$ and the basis vectors can be defined by

$$\cos\theta=\frac{F(i\alpha_2;\alpha_3)}{N(i\alpha_2;\alpha_3)} \ , \tag{2.3}$$

where N is the norm of the basis vector, i.e.,

$$N^2(i\alpha_2;\alpha_3)=\langle0|[\alpha_i^+\Gamma^+(\alpha_2)]_{\alpha_3}^\dagger[\alpha_i^+\Gamma^+(\alpha_2)]_{\alpha_3}|0\rangle \ . \tag{2.4}$$

The quantities $\cos\theta$ play the same role as the wave-function amplitudes in an orthonormal basis. They specify the structure of the calculated physical states $|\alpha_3\rangle$.

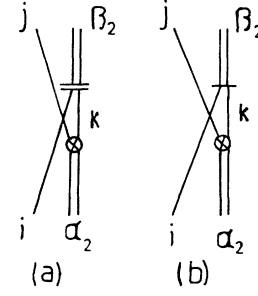The dynamical equations for the 3qp excitations can be derived by using the graphical procedure described in

FIG. 1. Graphical representation of (a) the Hamiltonian matrix and (b) the overlap matrix corresponding to the three-quasiparticle system. The double bar vertex represents the quantity $\Lambda(ik;\beta_2)$ in Eq. (2.5), the one bar vertex represents the projection F [as in Eq. (2.2)], the crossed circle vertex is the wave function amplitude X which, in this case of two-quasiparticle excitations (where the basis is orthonormal), coincides with the one bar vertex.

Ref. [11]. Even the overlap matrix among the basis vectors can be evaluated using that procedure. In our case the graphs corresponding to the dynamical and overlap matrices are very similar to each other, as seen in Fig. 1. The only difference is that the double bar vertex from Fig. 1(a), which has the value [11]

$$\Lambda(ik;\beta_2)=[\omega(\beta_2)-E_i-E_k]X(ik;\beta_2) \ , \tag{2.5}$$

is replaced in Fig. 1(b) by the one bar vertex, which is just $X(ik;\beta_2)$. From Fig. 1(a) one can write the dynamical equation as

$$\omega(\alpha_3)F(i\alpha_2;\alpha_3)=[E_i+\omega(\alpha_2)]F(i\alpha_2;\alpha_3)+\sum_{j\beta_2}\sum_k[\omega(\beta_2)-E_i-E_k]A(i\alpha_2,j\beta_2;k)F(j\beta_2;\alpha_3) \tag{2.6}$$

where, with standard notations,

$$A(i\alpha_2,j\beta_2;k)=\hat{\alpha}_2\hat{\beta}_2\begin{Bmatrix}i & k & \beta_2\\ j & \alpha_3 & \alpha_2\end{Bmatrix}x(kj;\alpha_2)x(ki;\beta_2) \tag{2.7}$$

and $x(ij;\alpha_2)=\sqrt{1+\delta_{ij}}X(ij;\alpha_2)$.

For the overlap matrix one obtains from Fig. 1(b) a similar expression

$$\langle0|[\alpha_j^+\Gamma^+(\beta_2)]_{\alpha_3}^\dagger[\alpha_i^+\Gamma^+(\alpha_2)]_{\alpha_3}|0\rangle=\delta_{ij}\delta_{\alpha_2\beta_2}+\sum_k A(i\alpha_2;j\beta_2;k) \ . \tag{2.8}$$

One can see that the dynamical equation and the overlap matrix for the 3qp excitations can be evaluated simultaneously. The QMSM building blocks contained in these equations are the one- and two-quasiparticle quantities, which have been calculated in the previous steps of the QMSM. In general, the blocks used in a given step are assumed to be taken from previous steps of the calculation. The suitability of these blocks is assured by comparing with the corresponding experimental data. Even more, one can often take the building blocks directly from experiment. This "renormalization" of theoretical

values has long since been used with great success in shell-model calculations [14,15].

III. NUMERICAL RESULTS AND DISCUSSIONS

The formalism presented above will be applied to calculate 3qp states in odd-even lead isotopes. The two-body interaction matrix elements were taken from Ref. [16] with some suitable changes, as described in Ref. [12], where it was found that in ^{194}Pb a sudden deviation of the predicted 2_1^+ and 4_1^+ energies appears. This was ascribed

to the influence of the intruder two-particle–two-hole proton excitations [12]. To avoid these complications we present here only applications for odd-even isotopes with $A \geq 197$.

In the first step we calculate the one-quasiparticle states. For the single-particle energies we use the experimental values given in Ref. [16]. The results for 1qp energies are plotted in Fig. 2.

In the next step we calculate the 2qp states by means of the QRPA as described in the preceding section. In particular, we neglect the backward-going components and normalize according to the TDA metric. The calculated spectra are in good agreement with experimental data, as shown in Ref. [12].

With the one- and two-quasiparticle states thus calculated we proceed to calculate the 3qp excitations within the QMSM basis (2.1). For this we evaluate the Hamiltonian matrix (2.6), which is not Hermitian, and the overlap matrix (2.8). We then use the Schmidt procedure to construct an orthonormal basis and evaluate within this basis the corresponding Hermitian dynamical matrix (for details of this procedure see Ref. [12]). Since we make approximations (like truncating the basis or neglecting QMSM vectors with small norm, i.e., vectors that are strongly suppressed by the Pauli principle), the dynamical matrix in that orthonormal basis may not be exactly Hermitian. We actually used this feature to check our approximations. The departure from hermiticity of the final dynamical matrix gives a measure of the adequacy of our approximations. Usually the calculated vectors are contained in very small QMSM subspaces. As we will see, this is true even in the case of 3qp states. This not only reduces the calculation efforts but also allows one to compare with more intuitive methods, like the weak coupling model.

In Fig. 3 we present the results of the calculation corresponding to high spin states in ^{197}Pb for which there are experimental data to compare with. To facilitate the analysis we also present the spectra of adjacent even-even isotopes. As seen in this figure the experimental spectrum is well reproduced by the calculation. The largest deviations appear for the states $21/2^-$ and $25/2^+$. The state $21/2^-$ is mainly a superposition of the QMSM basis vectors $5^- \otimes i_{13/2}$ and $12^+ \otimes p_{3/2}$. The projections $(\cos\theta)$ of the physical state with those two basis vectors are 1.22 (0.99) and 0.92 (0.92), respectively. We found that the rather large energy difference between the calculated and experimental level $21/2^-$ is due to the corresponding difference for the level 5^- in the adjacent even-even isotopes, as seen in Fig. 3. The two most important QMSM basis vectors to describe the level $25/2^+$ are $6^+ \otimes i_{13/2}$ and $9^- \otimes f_{7/2}$. The projections of these states upon the physical vector are 0.96 and 0.86, respectively. Since the experimental value of the energy corresponding to the state 6^+ is not available, it is not clear how much this two-quasiparticle state is responsible for the difference between the calculated and experimental energies of the state $25/2^+$ in ^{197}Pb. In spite of these differences, one can say that the agreement between theory and experiment in Fig. 3 is very good.

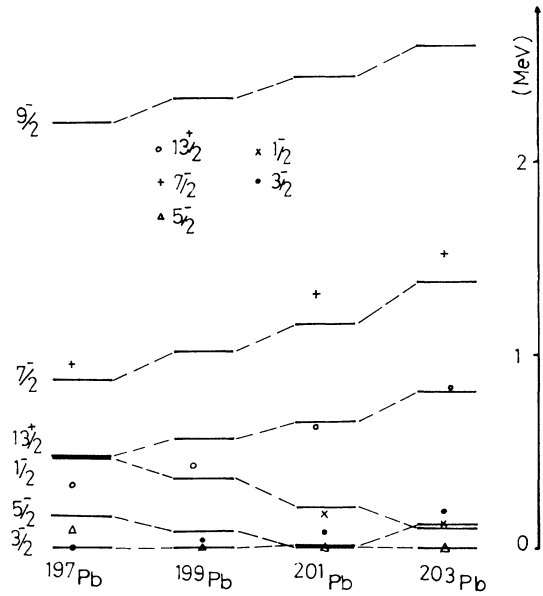A similar agreement can be seen in Figs. 4–6 corre-

FIG. 2. One-quasiparticle energies in odd-even lead isotopes. Full lines are the calculated levels. Experimental data are from Refs. [6–9].
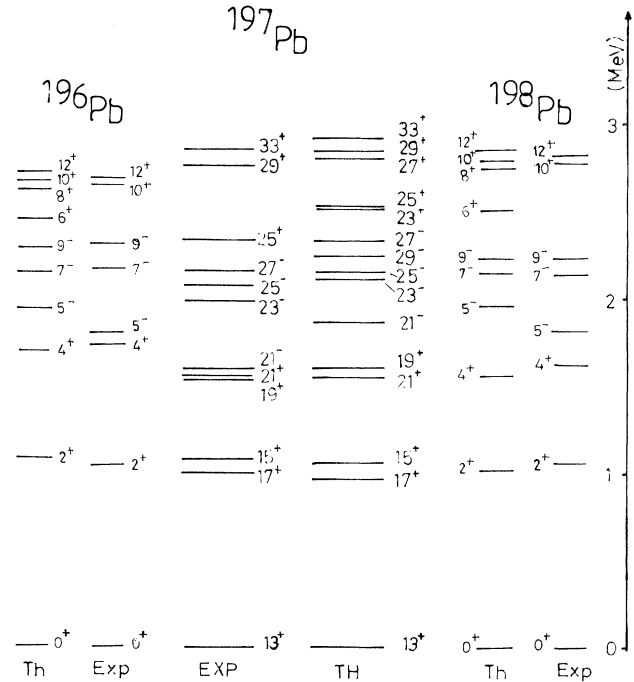

FIG. 3. Experimental [6] and theoretical three-quasiparticle states in ^{197}Pb. The experimental [17] and calculated levels corresponding to ^{196}Pb and ^{198}Pb are also given. In ^{197}Pb spins are doubled and energies are referred to the single quasiparticle state $i_{13/2}$.
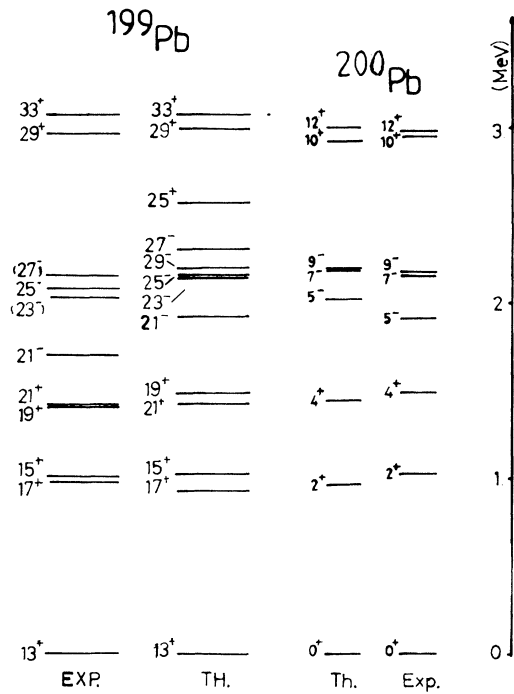
FIG. 4. As in Fig. 3 for ^{199}Pb. Here only one adjacent even-even spectrum is given. Experimental data are from Refs. [7] and [17].
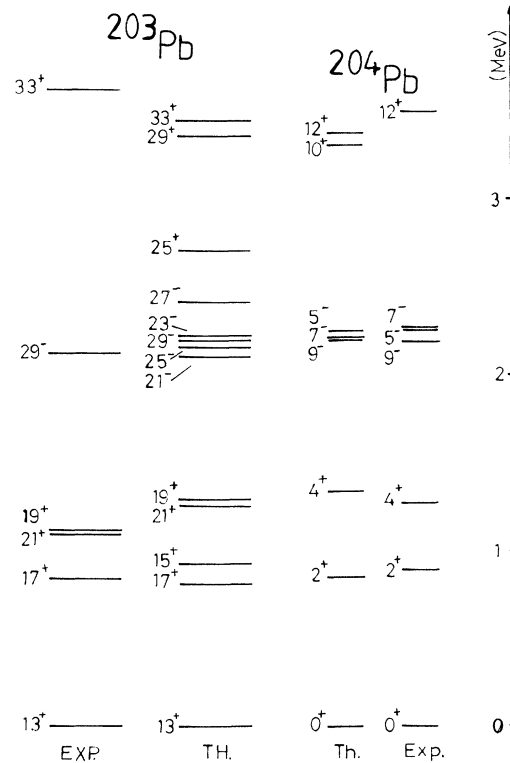

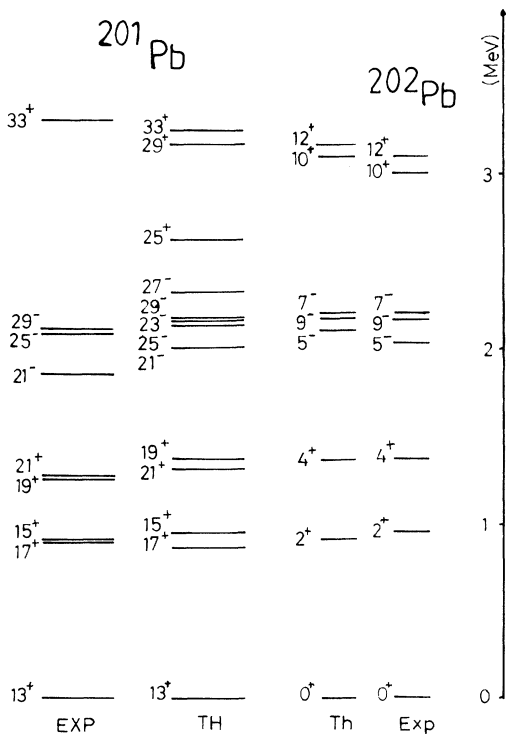FIG. 6. As Fig. 3 for ^{203}Pb. Experimental data are from Refs. [9] and [17].

FIG. 5. As in Fig. 4 for ^{201}Pb. Experimental data are from Refs. [8] and [17].

sponding to the nuclei ^{199}Pb–^{203}Pb. The differences between theory and experiment in Figs. 4–6 are about the same as in Fig. 3 and the causes of these differences are also the same.

To have a clear view of the general trends followed by the energy levels in odd lead isotopes, we present in Fig. 7 the theoretical and experimental energies as a function of the mass number A. The tendencies of the levels shown in Fig. 7 are similar to that corresponding to 2qp states, as seen in Fig. 8, indicating that the structure of the 3qp states is similar to the one corresponding to 2qp states. This can be understood by noting that high spin states are recombinations of a few single quasiparticle states. Thus, the states $29/2^+$ and $33/2^+$ in Fig. 7(a) have both the simple shell-model structure $(i_{13/2})^{-3}$ and, therefore, in the corresponding QMSM description the states 10_1^+ and 12_1^+ play a fundamental role. Similarly the groups of levels $(15/2^+, 17/2^+)$, $(19/2^+, 21/2^+)$, and $(23/3^-, 25/2^-, 27/2^-)$ are dominated by the QMSM basis vectors $2^+ \otimes i_{13/2}$, $4^+ \otimes i_{13/2}$, and $7^- \otimes i_{13/2}$, respectively. Even more, as we mentioned before, the basis state $5^- \otimes i_{13/2}$ determines the behavior of the level $21/2^-$, which explains the similarities among these levels and the levels 5^- in Figs. 7 and 8, respectively. This feature is repeated in all cases where there are similarities in the tendencies of Figs. 7 and 8.

The overcompleteness of the QMSM basis can be illustrated by the level $29/2^-$ which is a superposition of two almost parallel basis vectors, $9^- \otimes i_{13/2}$ and $12^+ \otimes f_{5/2}$.

Since the levels 7^- and 9^- have the same shell-model structure their behavior is the same as the one corresponding to the states $29/2^-$, as also can be seen in Figs. 7 and 8.

Because the first 2^+ state is well separated from other states, one expects, according to the weak coupling model, to identify a multiplet structure in this region. In Fig. 9 we present the multiplet $2^+ \otimes i_{13/2}$ in ^{197}Pb calculated within different QMSM subspaces. One sees in Fig. 9 that a large splitting among the constituents of the multiplet develops as the dimension of the QMSM subspace increases. Moreover, in the calculation performed within the large QMSM basis one notices that the vector $p_{3/2} \otimes 5^-$ is important to describe the state $13/2^+$ in Fig.

FIG. 8. (a) Theoretical 2qp energies in even-even lead isotopes as a function of the mass number A. (b) Experimental [23] low-lying energies in even-even lead isotopes as a function of the mass number A.
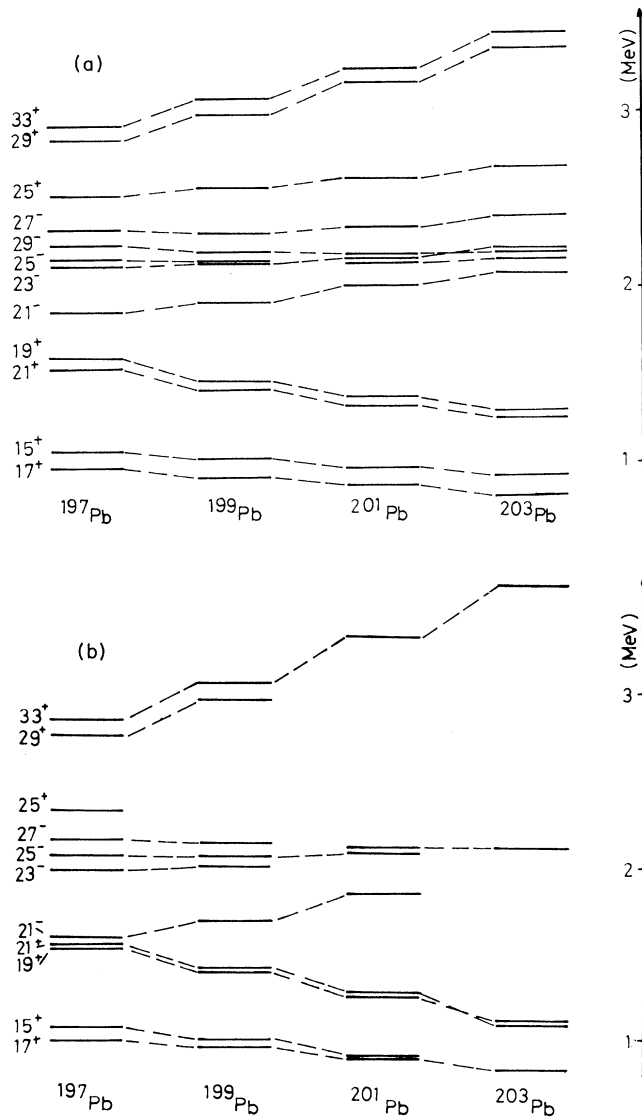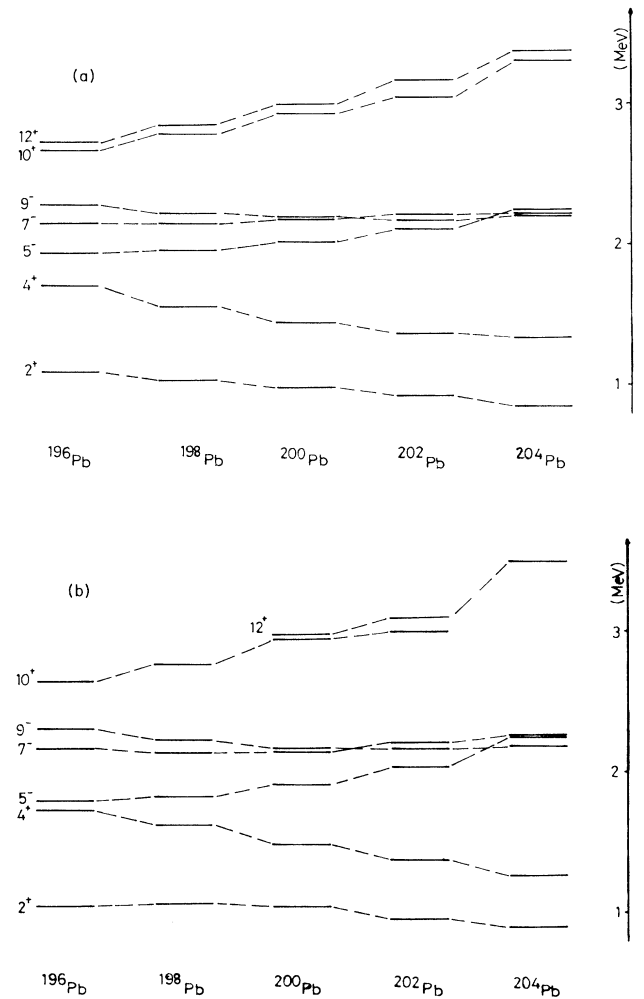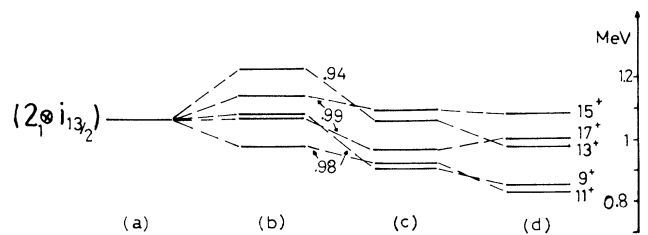

FIG. 7. (a) Yrast high spin 3qp states calculated in odd-even lead isotopes as a function of the mass number A and (b) the corresponding experimental values [6–9]. Spins are doubled and energies are referred to the states $i_{13/2}$.

FIG. 9. The multiplet $(2^+ \otimes i_{13/2})$ in ^{197}Pb corresponding to (a) zeroth-order QMSM basis vector, (b) QMSM calculation in a one-dimensional basis, and (c) QMSM calculation within a 40-dimensional basis. In (d) the experimental energies [6] are given. The numbers attached to the lines joining the main components of the physical vectors are the values of $\cos\theta$. The energies are referred to $i_{13/2}$ and the spins are doubled.
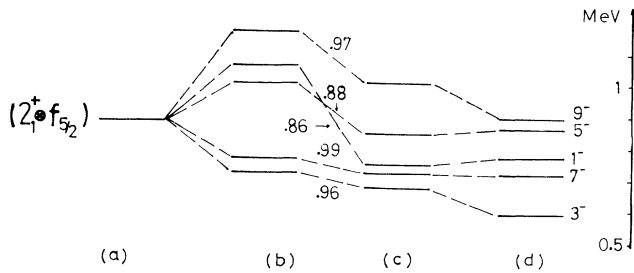
FIG. 10. As in Fig. 9 for the multiplet $(2^+ \otimes f_{5/2})$ in ^{203}Pb. The energies are referred to $f_{5/2}$ and experimental data are from Ref. [9].

FIG. 11. The wave function amplitudes for the states 2_1^+ in even-even lead isotopes as a function of mass number A. Only amplitudes in absolute value larger than 0.2 are plotted.

9. In particular the energy of the state $13/2^+$ is lowered due to the influence of that basis vector.

As another example we show in Fig. 10 the multiplet $2^+ \otimes f_{5/2}$ in ^{203}Pb [9]. In this case the one vector approximation implied by the weak coupling model reproduces rather poorly the experimental data. It is worth pointing out that for the states $1/2^-$ and $9/2^-$ the QMSM basis vector $2^+ \otimes f_{5/2}$ has small norms (0.77 and 0.62, respectively) as expected from the structure of the states 2_1^+ shown in Fig. 11. As a result the state $1/2^-$ in Fig. 10 has the largest projection with the QMSM vector $2^+ \otimes p_{3/2}$, in contradiction with the weak coupling model.

We have also verified that the convergence of the QMSM calculation as the dimensions are increased is good. Thus including only the two or three basis vectors with the largest overlaps with the physical state, one obtains virtually the same results as those with full dimensions.

IV. SUMMARY AND CONCLUSIONS

In this paper we have analyzed three-quasiparticle excitations in the odd-mass lead isotopes $197 \leq A \leq 203$ within the framework of a quasiparticle multistep shell-model method (QMSM). In the first step of the calculation one evaluates the quasiparticle quantities (e.g., occupation probabilities) starting with a "realistic" [16] interaction. In the second step one calculates two-quasiparticle excitations by using a quasiparticle RPA. One thus isolates the spurious 0^+ state that appears as a result of the breaking of the number of particles (gauge) symmetry. In the last step of the calculation the QMSM basis vectors are constructed as the tensor product of one times two-quasiparticle states. The spuriosity mentioned above is avoided by excluding the 0_1^+ two-quasiparticle state in the basis while the violations of the Pauli principle as well as the overcounting of independent states are corrected by evalu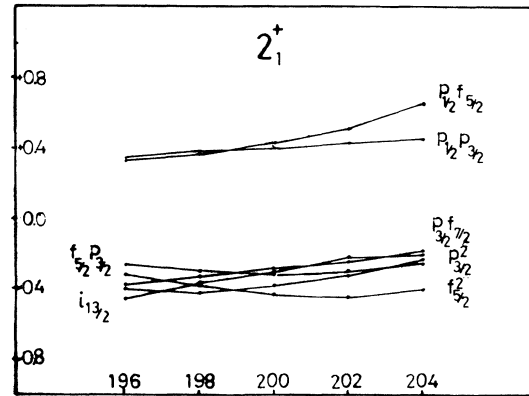ating the overlap matrix among the basis vectors. Since the backward-going QRPA amplitudes are negligible we exclude them from our calculation. As a result our three-quasiparticle formalism is of a TDA form, i.e., the metric is the normal geometrical metric. This allows us to define "angles" among vectors, in particular the angle θ between the physical vector and a given QMSM basis vector. The value of $\cos\theta$ is the equivalent of the wave-function amplitude in a formalism that uses orthonormal basis (like the standard shell model).

The results of the calculation agree well with the corresponding experimental data. We found that usually only few QMSM basis vectors are important to describe the physical states. In most cases only one basis vector is enough to describe reasonably well the yrast states. This explains the similarities between the yrast spectra of two- and three-quasiparticle levels found in lead isotopes.

For the isotopes ^{197}Pb and ^{203}Pb we have presented the evolution of the states belonging to the multiplets $(2_1^+ \otimes i_{13/2})$ and $(2_1^+ \otimes f_{5/2})$ as a function of the basis dimension. We found that the members of these multiplets are often strongly mixed with other QMSM components thus limiting the validity of the weak coupling model.

This work completes the QMSM analysis of two- and four-quasiparticle excitations in lead isotopes started in Ref. [11]. We thus hope to have accomplished a unified QMSM description of even-even and odd-even lead isotopes, in which the states calculated in a given nucleus are building blocks for the calculation of other nuclei.

[1] J. Vanhorenbeeck et al., Nucl. Phys. A531, 63 (1991).
[2] M. Pautrat et al., Nucl. Phys. A484, 155 (1988).
[3] M. Pautrat, M. Lagrange, J. S. Dionisio, Ch. Vien, and J. Vanhorenbeeck, Nucl. Phys. A443, 172 (1985).

[4] H. Helppi et al., Phys. Rev. C 23, 1446 (1981).
[5] H. Richel et al., Z. Phys. A 284, 425 (1978).
[6] Zhou Chunmei, Nucl. Data Sheets 62, 433 (1991).
[7] M. R. Schmorak, Nucl. Data Sheets 53, 331 (1988).

[8] M. R. Schmorak, Nucl. Data Sheets **49**, 733 (1986).

[9] M. R. Schmorak, Nucl. Data Sheets **46**, 287 (1985).

[10] T. T. S. Kuo, E. U. Baranger, and M. Baranger, Nucl. Phys. **79**, 513 (1966).

[11] R. Arvieu, O. Bohigas, and C. Quesne, Nucl. Phys. **A143**, 577 (1970).

[12] C. Pomar, J. Blomqvist, R. J. Liotta, and A. Insolia, Nucl. Phys. **A515**, 381 (1990).

[13] R. J. Liotta and C. Pomar, Nucl. Phys. **A382**, 1 (1982).

[14] N. Auerbach and I. Talmi, Nucl. Phys. **64**, 458 (1965).

[15] C. G. Lindén, I. Bergström, J. Blomqvist, K.-G. Rensfelt, H. Sergolle, and W. Westerberg, Z. Phys. A **277**, 273 (1976).

[16] T. T. S. Kuo and G. H. Herling, Naval Research Laboratory Report No. 2258 (NRL, Washington, D.C., 1971); G. H. Herling and T. T. S. Kuo, Nucl. Phys. **A181**, 113 (1972).

[17] J. Halperin, Nucl. Data Sheets **28**, 485 (1979); Zhou Chunmei, *ibid.* **60**, 527 (1990); M. R. Schmorak, *ibid.* **51**, 689 (1987); **50**, 669 (1987); **50**, 719 (1987).